Groundwater

Advective Transport Phenomena to Better Understand Dispersion in Field and Modeling Practice

by Willem J. de Lange[1]

Abstract

The absence of recent research on dispersion in engineering applications indicates the need for a description that is more focused on field and modeling practice. Engineers may benefit from simple calculation tools allowing them to understand the processes encountered in the field. Based on a conceptual model for advective transport through an elongated conductivity zone, for example, in fluvial sediments, explicit expressions are presented for macro-scale phenomena: (1) the different travel distances of water particles traveling in laminar flow through and adjacent to a single zone with conductivity higher or lower than that of the aquifer; (2) the affected thickness of the bundle of flowlines; (3) the distinction of inflow, outflow, and through-flow sections; (4) the development of a plume front vs. that of a tail; (5) conservation of mass causing water particles to travel both slower and faster than the aquifer average velocity while passing a single zone. The spread derived from a spatial distribution in a field experiment relates to the geometric mean of the spreads of the plume front and tail. The results obtained for a single conductivity zone are expanded for a general aquifer that is characterized by stochastic parameters. A fundamental new expression describes the dispersive mass flux as the product of the advective volume shift and the related local concentration difference. Contrary to Fickian theory, the dispersive mass flux in both the front and tail of a plume in highly heterogeneous aquifers is limited. In modeling, the advective volume shift is proportional to the cell size.

Introduction

Recent discussions (Hadley and Newell 2014; Neuman 2014; Molz 2015) show the need for a better understanding of dispersion phenomena in field experiments and modeling practice. Although stochastic theory and research modeling has been strongly developed over the years (Neuman and Tartakovsky 2009; Fiori et al. 2017), most is not applied in engineering practice (Fiori et al. 2016). Applications of transport modeling generally stick to Fickian theory combining dispersivity with the local concentration gradient as described in the manual by Zheng and Wang (1999) and in the handbooks from Bear and Verruijt (1987), Appelo and Postma (1993), and Batu (2006). Dual domain concepts (Feehley et al. 2000) are rarely used in practice. Insights obtained from research modeling by Jankovic et al. (2003) and Fiori et al. (2006, 2013) on the role of advective transport at macro scale has not yet landed in applied modeling. It is also well known that the concentration gradient is not the driving force for dispersion (Konikow 2011) but is still interpreted as such. Molz (2015) mentions that fieldworkers need a realistic concept of transport in groundwater. Engineers may benefit from simple expressions to better understand dispersion phenomena encountered in the field before considering a significant modeling effort such as needed for stochastic simulations (Fiori et al. 2016). Hadley and Newell (2014) quote Theis (1967) mentioning that "... we need a new conceptual model, containing the known heterogeneities of natural aquifers to explain the phenomenon of transport in groundwater." Fiori et al. (2013) modeled explicit geological features in combination with local dispersion in the highly heterogeneous aquifer at the MADE test site. They conclude that "local advection and the conductivity spatial variability are apparently the only mechanisms needed to explain and predict the MADE findings."

[1]Corresponding author: Deltares Unit Subsurface and Groundwater Systems, P.O. Box 85467, 3508 AL, Deltares, Utrecht, The Netherlands; wim.delange@deltares.nl

Article impact statement: Simple expressions to explain differences in dispersion parameters between field and modeling practice based on advective transport.

Received September 2018, accepted March 2019.

doi: 10.1111/gwat.12883

In these footsteps, the present work shows that longitudinal dispersion can be generated by advective transport phenomena that are fundamentally different from diffusive dispersion as described by Fick's law.

The macroscale phenomena addressed are the following: (1) the different travel distances of water particles traveling in laminar flow through and adjacent to a single zone with conductivity different from that of the aquifer; (2) the thickness of the bundle of flowlines that is affected by such a single conductivity zone; (3) the inflow, outflow, and through-flow sections distinguished in such a zone; (4) the differences in the development of a plume front vs. that of a tail; (5) conservation of mass causing water particles to travel both slower and faster than the aquifer average velocity while passing a single zone.

The phenomena are explored in aquifers characterized by horizontal conductivity zones of limited extent, as encountered in fluvial sediments. Along the main direction of groundwater flow, water particles travel with different velocities while passing different conductivity zones. This process is observed in a vertical section along a flow line.

In the first step, we observe the deformation of a front of water particles as it passes through a single conductivity zone in a homogeneous aquifer. The front is deformed over a length (spread) and thickness (wake) which are described by simple expressions that include the dimensions and conductivities of the aquifer, the zone, and the thickness of the observed plume (if known).

The second step expands this single zone concept for an aquifer defined by stochastic parameters. The spread and wake of the deformation are used to determine the advective volume shift, a fundamental new parameter for dispersion in groundwater. The dispersive mass flux equals the product of the advective-volume shift and the local mass gradient.

Issues relevant for modeling and field practice are: (1) the differences in the spread of the front and the tail of a plume; (2) the impact of a plume being thin; (3) the differences in dispersed mass between a Fickian and advective process; (4) the new dispersion parameter, the advective volume shift, being proportional to the cell size.

The present work elaborates on previous research by Eames and Bush (1999) and Dagan and Lessoff (2001) who derived expressions for dispersion of water particles flowing through multiple circular and elliptic inclusions with a bimodal conductivity distribution in a homogeneous aquifer. Fiori et al. (2003) and Jankovic et al. (2003) expanded the analysis by using two-dimensional (2D) and three-dimensional (3D) models with thousands of inclusions.

Figures 1 and 3 show flow lines in vertical cross section and are generated with analytic elements (Strack 1989) by using line-doublets for the boundary of the zone and line-dipoles for the aquifer boundary at top and bottom.

Expressions for Water Particles Flowing through a Single, Elongated Zone

Case Description

We will explore the phenomena in theory and quantity by means of a case study with a single elongated zone with conductivity higher (but can be lower) than that of the aquifer (Figure 1). The parameter values and dimensions occur in fluvial sediments such as those found in sandpits in the Netherlands (W. Westerhof 2009), Germany (Heinz and Aigner 2003), and the MADE aquifer (Rehfeld et al. 1992, Figure 7).

Figure 1 shows flow lines in blue and equipotential lines in green. The predominantly horizontal conductivity zone or heterogeneity (index h) has a length $L_h = 29$ m and a thickness $D_h = 0.8$ m with a conductivity $k_h = 10$ m/d that is 10 times higher than that of the aquifer (index a) $k_a = 1$ m/d. In the aquifer, with thickness $D_a = 12.5$ m, the heterogeneity is essentially parallel to the virtually horizontal bulk flow in the aquifer.

The Spread of Water Particles Caused by Flowing through a Single Conductivity Zone

The spread (Δs [m]) is defined as the change in travel distance (s [m]) after passing though the conductivity zone where water particles return to the same horizontal position as they were prior to entering the conductivity zone. Water particles traveling in the conductivity zone are shifted forward (or backward in case of a low conductivity zone) with respect to water particles in the aquifer. The spread of water particles after passing through the conductivity zone can be quantified by integrating the difference of the advective velocities [m/d] along flow lines inside (v_h) and outside (v_a) the zone over a time T [d]:

$$\Delta s = \int_T [v_h(s) - v_a(s)]\, dt \tag{1}$$

The time (T) needed for a particle to travel over the length (L_h) inside the zone is expressed by:

$$\int_T dt = \int_{L_h} \left[1/v_h(s)\right] ds \tag{2}$$

Combination of Equations 1 and 2 leads to

$$\Delta s = \int_{L_h} \frac{[v_h(s) - v_a(s)]}{v_h(s)}\, ds \tag{3}$$

The particle velocity v_i in the aquifer (i = a) and inside the zone (i = h) is expressed by:

$$v_i(s) = -k_i/n_i^* \partial\phi_i/\partial s \quad (i = a, h) \tag{4}$$

Here, n is the porosity [−] and ϕ [m] is the head. Along the main part of the conductivity zone in Figure 1, the head gradient is about equal inside and outside. Neglecting the differences in the gradient, the velocity ratio becomes $v_a(s)/v_h(s) = (k_a/n_a)/(k_h/n_h)$. Substitution

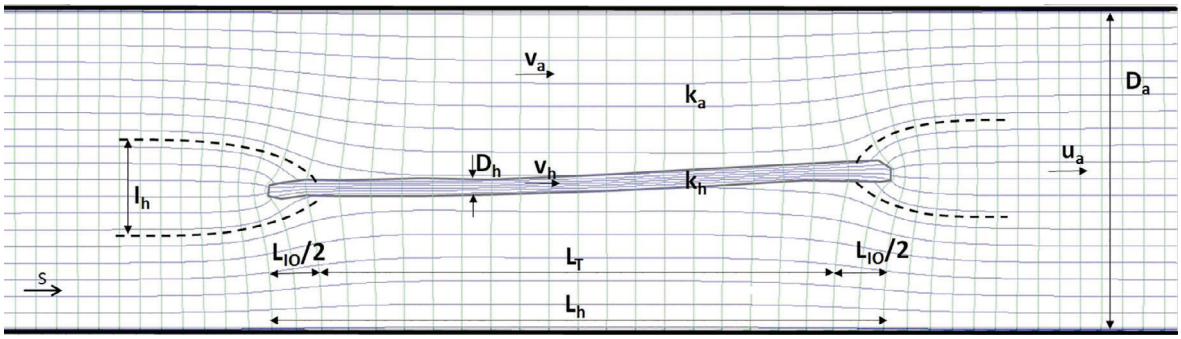

Figure 1. Vertical cross section: flow (blue) and equipotential (green) lines in the case of a high conductivity zone in a bounded aquifer.

in Equation 3 yields the following simple expression for the particle spread:

$$\Delta s = (1-\kappa/\eta)\ L_h \tag{5}$$

where $\eta = n_a/n_h[-]$ is the porosity ratio and $\kappa = k_a/k_h$ $[-]$ is the conductivity ratio that is the reciprocal to that presented in previous work (Eames and Bush 1999; Dagan and Lessoff 2001), which was defined as $\kappa^* = k_h/k_a$ $[-]$. Dagan and Lessoff (2001) mention a ratio of 8 for high conductivity and 1/100 for low conductivity when referring to κ^* values. In their Equation 15, the position of the conductivity ratio is similar to that of Equation 5 presented above, so κ $(=1/\kappa^*)$ should be used instead.

For a path length (s [m]) smaller than L_h, the spread follows from the linear growth inside the zone and can simply be calculated by replacing s for L_h in Equation 5. In the case of a low conductivity zone Δs can be larger than s. The latter is the physical maximum and replaces Δs in that case. In case of a high conductivity zone, Δs is limited to L_h.

Low and high conductivity values can be assessed as follows. In practice, the variation of the conductivity in the aquifer is ideally known by the stochastic parameter $\sigma^2_{\ln k}$ $[-]$. Figure 2 shows a log normal distribution with the conductivity ratio κ^* along the x-axis. The standard deviation $\sigma_{\ln k}$ may be considered to represent a high and a low value of κ^*.

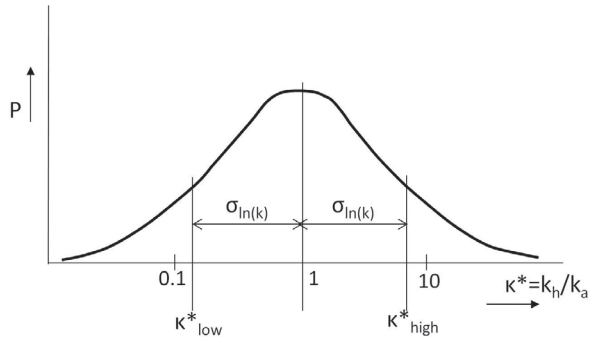

Figure 2. Schematic logarithmic probability distribution of $\kappa^* = k_h/k_a$ with κ^*_{high} and κ^*_{low} being the values at standard deviation.

Because $\sigma_{\ln k}$ is positive, it follows from Figure 2 that:

$$\sigma_{\ln k} = \ln\left(\kappa^*_{high}\right) - \ln(1) = \ln\left(\kappa^*_{high}\right) = \ln\left(1/\kappa_{high}\right) \tag{6a}$$

$$\sigma_{\ln k} = \ln(1) - \ln\left(\kappa^*_{low}\right) = -\ln\left(\kappa^*_{low}\right) = \ln(\kappa_{low}) \tag{6b}$$

The conductivity ratios κ_{high} and κ_{low} can be determined from $\sigma^2_{\ln k}$ by using:

$$1/\kappa_{high} = \kappa_{low} = e^{\left(\sqrt{\sigma^2_{\ln k}}\right)} \tag{7}$$

Implying that $\kappa_{high}\kappa_{low} = 1$, Equation 7 provides a straight forward relation between $\sigma^2_{\ln k}$ and the two values of κ representing zones with high and low conductivities. These two values can be attributed to the spread in the front (for zones with high conductivity) and in the tail (for zones with low conductivity).

The Wake of a Conductivity Zone

The vertical distance denoted by I_h [m] in Figure 1 covers the flow lines entering and leaving the conductivity zone and is called "the wake" after Eames and Bush (1999). The expression for I_h follows from considering continuity of flow in the undisturbed aquifer and at the center of the zone:

$$I_h u_a n_a = D_h v_h n_h \tag{8}$$

where, u_a [m/d] is the undisturbed uniform velocity in the aquifer (Figure 1). In the aquifer outside the wake, continuity of flow yields:

$$(D_a - I_h)\ u_a = (D_a - D_h)\ v_a \tag{9}$$

Combining Equations 8 and 9, rewritten as the ratio of u_a/v_h and using Equation 4 as in the derivation of Equation 5 yields the expression for the wake:

$$I_h = D_a/\left[1 + \kappa\,(D_a/D_h - 1)\right] \tag{10}$$

By this expression, the thickness over which a plume front is distorted by passing through a single high-conductivity zone is determined. For the case described above, the resulting value $I_h = 5.08$ m agrees well with I_h depicted in Figure 1. Typical relationships that may be found are $I_h = D_h/\kappa$ for zones of low conductivity ($\kappa >> 1$), $I_h = D_h$ for weakly heterogeneous aquifers ($\kappa \approx 1$) and $I_h = D_a$ for zones of high conductivity ($\kappa << 1$). This latter limitation to I_h implies a limitation of the flux in a high-conductivity zone and so to a limitation of the velocity inside. The wake does not depend on the porosity ratio as it describes mass conservation rather than particle spread. This is also mentioned by Lessoff and Dagan (2001).

Particle Spread during In/Outflow vs. Plume Shift during Through-Flow

The flow lines (Figure 1) contract and expand near the tips of the conductivity zone in the so-called "inflow and outflow sections" with the combined length L_{IO} [m]. Between these sections the flow is virtually one-dimensional (1D) in the "through-flow section" L_T [m]. The length L_{IO} can be assessed in an "ideal" situation of unlimited flow into the conductivity zone in an infinite aquifer as derived by (De Lange 1996, equation 5.40). Adapted in this paper by using different symbols, it can be written as:

$$\eta\, u_a/v_h = D_h/L_{IO} + \kappa \tag{11}$$

This expression has been derived by inverse modeling and also can be derived from an analytical solution by Strack (1981). By combining Equations 8, 10, and 11 L_{IO} becomes:

$$L_{IO} = D_a/(1-\kappa) \quad \text{for } L_{IO} < L_h \tag{12}$$

The length of the through-flow section L_T (Figure 1) is described by:

$$L_T = L_h - L_{IO} \quad \text{for } L_{IO} < L_h \tag{13}$$

Using the values of the example case as input, calculated values for $L_{IO} = 13.89$ m and $L_T = 15.11$ m agree well with Figure 1. If $L_h \geq D_a/(1-\kappa)$ then a through-flow section establishes meaning in high conductivity zones that are longer than the thickness of the aquifer.

Water particles in adjacent flow lines are shifted relative to each other while crossing the boundary of the high-conductivity zone (Figure 1) causing spreading along the flow lines. In the inflow and outflow sections, water particles travel over different path lengths generating particle spreading in the plume. In the through-flow section, water particles travel parallel to each other with equal velocity. In this zone, the part of the plume that is captured in the wake is shifted as a whole relative to the water particles outside the wake, generating a so-called "block-shift." Inside the high conductivity zone, this part of the plume is also stretched due to the high velocity.

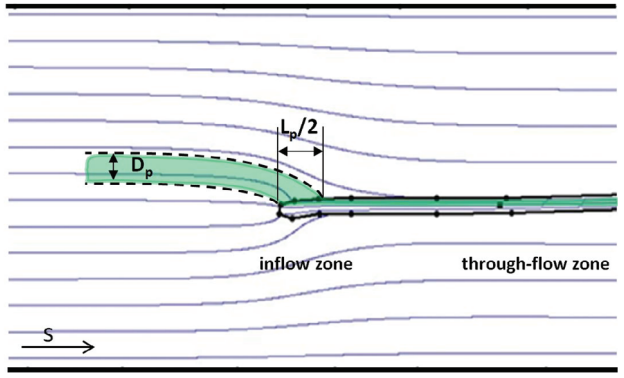

Figure 3. Vertical cross section: a thin plume entering the high conductivity zone of Figure 1.

Spreading of Thin Plumes

In field experiments such as those performed at Borden (Rajaram and Gelhar 1991), Cape Cod (Hess et al. 2002), and MADE (Adams and Gelhar 1992) the deformation of a plume has been measured in 3D along the travel path showing the thickness of the injected volume. In the cases where the plume thickness is thinner than the wake, the lengths of the inflow section (being half the length of the combined inflow outflow section) $L_p/2$ will be reduced (Figure 3).

The length (L_p) is assessed by using proportionality with the plume thickness (D_p) over the maximum thickness of flow lines that enter the conductivity zone, so the wake I_h:

$$L_p = \theta L_{IO} \quad \text{with} \quad \theta = D_p/I_h\ (\leq 1) \tag{14}$$

Using the values from the example case and $D_p = 1$ [m], the calculated values $L_p = 2.74$ m and $\theta = 0.20$ [−] agree well with Figure 3. The reduced spread of a plume thinner than the wake passing through a high conductivity zone results from using L_p instead of L_{IO} in Equation 5.

At test sites in Denmark (Jensen et al. 1993) and Horkheim (Ptak and Teutsch 1994), measurements in filters have been interpreted by using break-through curves. In the filters, only a "thin plume" is measured, that easily may by inside a conductivity zone. In a high (or low) conductivity zone, the plume is stretched (or compressed) as compared to when flowing in the undisturbed aquifer. This may cause an overestimation (or underestimation) of the spread or dispersion, which can be corrected by multiplying the spread by the ratio of velocities in the undisturbed aquifer (u_a) and in the zone (v_h) as follows from Equations 8 and 10:

$$\frac{u_a}{v_h} = \frac{D_h}{I_h \eta} = \frac{D_h}{D_a}\frac{(1-\kappa)}{\eta} + \frac{\kappa}{\eta} \tag{15}$$

In the example case of Figure 1 the ratio equals 0.16, which is significant. The scaling of Equation 15 is different from using the conductivity ratio (κ) as often done in practice.

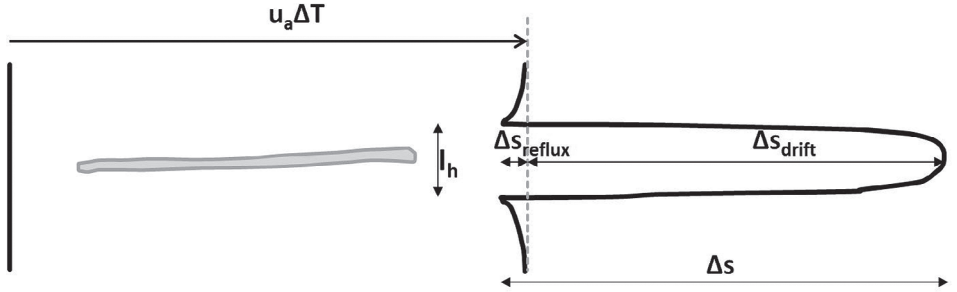

Figure 4. Calculated deformation of a water particle front after passing the conductivity zone of Figure 1.

Forward Shift (Drift) vs. Lagging Behind (Reflux)

Figure 4 shows the simulated deformation of a straight vertical front of water particles after passing through the conductivity zone of Figure 1. The shape of the deformation is similar to that obtained by Dagan and Lessoff (2001) in the case with an ellipsoidal inclusion.

The water particles inside the wake (I_h in Figure 4) have been shifted forward and those outside lagged behind compared with the aquifer-average displacement (vertical dashed line in Figure 4). Eames and Bush (1999) call the flow in these zones, the drift and the reflux, respectively. The spreads caused by the drift (Δs_{drift} [m]) and the reflux (Δs_{reflux} [m]) follow from the velocities of v_h and v_a relative to u_a (see Figure 1). Using Equations 2, 8, and 10 these spreads become:

$$\Delta s_{drift} = \left(1 - \frac{\kappa}{\eta}\right) * \left(1 - \frac{D_h}{D_a}\right) L_h \qquad (16)$$

and

$$\Delta s_{reflux} = \left(1 - \frac{\kappa}{\eta}\right) * \frac{D_h}{D_a} L_h \qquad (17)$$

The ratio between these shifts $\Delta s_{drift}/\Delta s_{reflux} = D_a/D_h - 1$ does not depend on κ/η or L_h because it describes mass conservation. The closed mass balance of this phenomenon is expressed by $\Delta s_{drift} D_h = -\Delta s_{reflux}(D_a - D_h)$. The back shift is significant in cases where heterogeneities fill up a significant part (>30%) of the aquifer thickness. The distinction between drift and reflux also applies in the case of low conductivity heterogeneities but in directions opposite to those in Figure 4.

Using values from the case of Figure 1, the calculated values for $\Delta s_{drift} = 24.43$ m and $\Delta s_{reflux} = 1.67$ m are smaller than occurring in Figure 4. This is due to the spread of water particles occurring along the contracting flow lines just outside the conductivity zone. Simulations suggest that this length is about equal to I_h both for the inflow and outflow sections. The adapted spread in Equation 5 Δs $(L_h + I_h) = 35.24$ m is closer to the result of the analytic element simulation in Figure 4. This correction can immediately be applied to the previous expressions. Future research may result in additional corrective terms.

Expressions for a Heterogeneous Aquifer

Expansion to a Stochastic Characterized Aquifer

Next, the results obtained above for a single conductivity zone will be expanded for a general aquifer. This is done in two steps: (1) We show the similarity between the spread Equation 5 and the standard deviation of a particle distribution derived from the expression of (Gelhar and Axness 1983) for the classic dispersivity. (2) The expressions for a single zone are applied in a specified domain that is repeated to fill up the general aquifer, while the parameters applying to a single conductivity zone are replaced by stochastic parameters applying to the general aquifer.

Similarity between the Expressions for the Spread (Single Conductivity Zone) and for the Standard Deviation from Classic Dispersivity (General Aquifer)

In applied transport modeling, the (longitudinal) dispersivity (α [m]) is used in a Fickian expression for the mass flux. Gelhar and Axness (1983) relate α to the log conductivity variance (σ^2_{lnk}) and the characteristic length (I_y [m]) pertaining to the structure of the aquifer. We combine their expression (using $\lambda = 1$ [−] in their convention) with the general relation between the dispersivity and the variance ($\sigma_\alpha{}^2$ [m^2]) of the particle distribution at travel distance (s) to:

$$\alpha = \sigma^2_\alpha(s)/2s = \sigma^2_{lnk} I_y \qquad (18)$$

The characteristic length I_y is the radius of a zone around an observation point over which conductivity is related to the value at that point. In 2D space, the length of the conductivity zone L_h equals $2I_y$, which is in the footsteps of Fiori et al. (2003). Using this equality, the last two terms in Equation 18 can be rewritten into:

$$\sigma_\alpha(s) = \sqrt{(\sigma_{lnk} L_h)}\sqrt{(\sigma_{lnk} s)} \qquad (19)$$

The standard deviation following from classic dispersivity (σ_α) equals the geometric mean of two others. The first term ($\sigma_{lnk} s$) increases with travel distance similar to the spread of a tail as explained with Equation 5, while the second term ($\sigma_{lnk} L_h$) is limited with travel distance similar to the spread of the front a plume also explained with Equation 5, in a strongly heterogeneous aquifer. The

variance ($\sigma_\alpha{}^2$) can be interpreted as the product of the standard deviations or the spreads of the front and tail of the plume. Such a variance has been determined from the 3D particle distribution in field experiments such as those at Borden (Rajaram and Gelhar 1991), Cape Cod (Hess et al. 2002), and MADE (Adams and Gelhar 1992).

For weakly heterogeneous aquifers ($\sigma_{\ln k} < 1$), we may write:

$$\sigma_{\ln k} = -\ln(\kappa) = -\ln(1-\chi) \approx \chi = (1-\kappa) \qquad (20)$$

Using this, the standard deviation Equation 19 after passing a single conductivity zone ($s = L_h$) in weakly heterogeneous aquifers becomes:

$$\sigma_\alpha(L_h) = (1-\kappa)\, L_h \qquad (21)$$

This expression for the standard deviation is similar to that for the spread Equation 5, except for the porosity ratio. This similarity supports the expansion described in the following section. The meaning of the spread in Equation 5 for a single zone is similar to that of the standard deviation in Equation 21 for an aquifer with multiple heterogeneities. For simplicity, Δs is used from now on for both situations.

Expressions for a General Aquifer Characterized by Stochastic Parameters

A general heterogeneous aquifer is represented by many sub-aquifers (Figure 5, top), each with a single high or low conductivity zone. Each sub-aquifer covers a "domain A" in which deformation of a particle distribution occurs as represented by the gray fronts in Figure 5 (bottom). All domains A's together generate a distribution of conductivity zones meant to be similar to that as used by Eames and Bush (1999), Dagan and Lessoff (2001), and Lessoff and Dagan (2001). In these studies, they derived expressions for the dispersivity from 2D integration of the local displacement in water particles passing through individual inclusions described by mathematical functions. Their inclusions are assumed not to interfere with respect to spreading. This is simplified in this study as stacked domain A's as sketched in the top image of Figure 5. Boundaries are created by horizontal flow lines between these domains. This complies with the impermeable top and bottom as sketched in Figure 1 generating independency of spreading in each domain.

The specification of domain A and the conductivity zone are based on the following.

Jankovic et al. (2003) used the stochastic parameters $\sigma^2{}_{\ln k}$ and I_y to parameterize the numerous circular and spherical inclusions in a homogeneous aquifer to represent a general heterogeneous aquifer. For weakly heterogeneous soils, their result [$\alpha = \sigma_{\ln k} N I_y$] is equal to Equation 18 except for the volume fraction of heterogeneities N. We use N to determine the dimensions of the periodic domain A by $L = L_h/N$ and $D = D_h/N$. In line with Equations 18 through 21, the result of Jankovic et al. (2003) means that the value of σ_α in a general aquifer can be calculated by using the stochastic values in Equation 21 as well as in Equation 5 as if there were properties for a single conductive zone. Vice versa, a single conductivity zone with stochastic parameter values may represent a heterogeneous aquifer with respect to the resulting spreading in each domain A in Figure 5. This is the basis of our "working model."

As described with Equation 19, the stochastic parameter I_y is directly related to L_h and the same applies to the vertical characteristic length I_z and D_h. The value of N can be assessed from the stochastic characterization of the aquifer or from expert knowledge of geologists and is assessed to range from 0.1 to 0.3 ($N \approx 0.16$ in the case of Figure 5). Using this and the expressions for L and D above, the dimensions of both the conductivity zone and domain A are directly related to stochastic parameters describing the general aquifer. The stochastic parameter $\sigma_{\ln k}$ leads to κ_{high} and κ_{low} with the use of Equation 7. The porosity ratio θ can be related to κ for instance by using Table 2.1 as presented in Dominico and Schwarz (1990). These stochastic parameters can be used in Equation 5 to compute the change in the standard deviation or spread of the particle distribution caused by dispersion *in each domain A*, by:

$$\Delta s_j\big|_A = \left(1 - \kappa_j/\eta_j\right) L_h \qquad (22)$$

In which j denotes the high or low conductivity and represents the front or tail of a plume. In our "working model," all zones are high-conductive when calculating spread of a front and low conductive when calculating spread of a tail.

Expressions for Dispersive Mass Transport

The bottom image of Figure 5 shows the computed distortion of a plume front in which all water particles have passed through the conductivity zone. In each domain A, the change of mass (ΔM) consists of a spread over the distance (Δs) of the water particles within the wake (I_h), with the concentration difference $\Delta c_A = (c_1 - c_0)$ yielding:

$$\Delta M_j\big|_A = \Delta c_A \;\; \Delta s_j\big|_A \;\; I_{h,j} \qquad (23)$$

where j is defined with Equation 22. This change of mass occurs during period T_A that is needed to pass length L at the average velocity in the aquifer. This leads to the dispersive mass flux (F_A) in domain A:

$$F_{A,j} = \frac{\Delta M_j\big|_A}{\Delta T_A} = \frac{\Delta M_j\big|_A}{L} u_a \qquad (24)$$

The specific dispersive mass flux (f) per unit volume becomes:

$$f_j = \frac{F_{A,j}}{A} = \frac{\Delta M_j\big|_A}{AL} u_a = \frac{\Delta s_j\big|_A}{L} \frac{I_{h,j}}{D} \frac{\Delta c_A}{L} u_a \qquad (25)$$

where j is defined in Equation 22. This expression represents the advective transport per unit volume in the

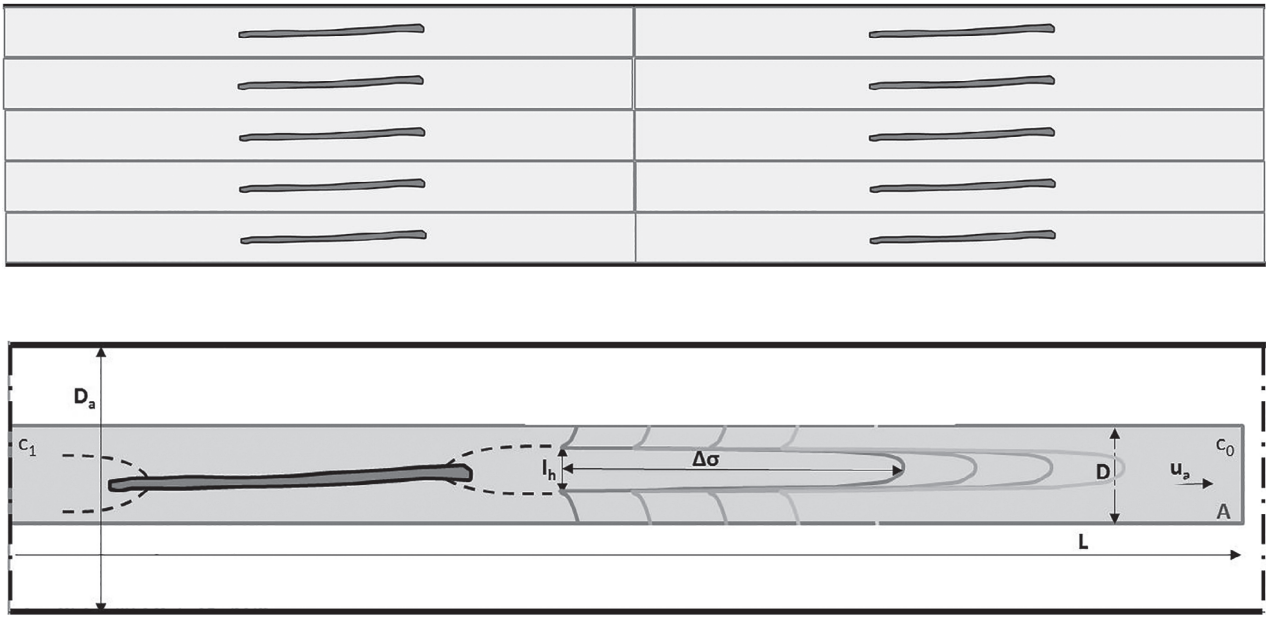

Figure 5. Vertical cross sections. Top: periodic domains filling up an aquifer; bottom: domain A (gray area) with a single conductivity zone.

general aquifer. The classic expression for longitudinal dispersion applies to the spreading of a plume in the equilibrium phase. In our case, this occurs to a plume after passing a complete domain A or distance L. In practice, the dispersive mass flux Equation 25 is transferred in a Fickian-like expression for the mass flux ($F_j|_L$) that is valid over any distance L. The unit concentration gradient follows from $\Delta c/\Delta x = \Delta c_A/L$ yielding:

$$F_j\big|_L = f_j\, L = \omega_j \frac{\Delta c}{\Delta x}\, u_a \tag{26}$$

where ω_j is called the *advective volume shift* expressed by:

$$\omega_j = \beta_j\ \ \Delta s_j\big|_A = \beta_j\ (1 - \kappa_i/\eta_i)\, L_h \tag{27}$$

Here β is the *wake fraction* I_h/D that can be reworked using Equation 8 with $D_a = D$ to*:*

$$\beta_j = I_{hj}/D = 1/\left[1 + \kappa_i\,(1/N - 1)\right] \tag{28}$$

The wake fraction (β) limits the dispersive mass of a long tail by accounting for the wake (I_h) being thin. For low conductivity ratios ($\kappa >> 1$) and if $N << 1$, Equation 28 simplifies to $\beta = -N/\kappa$. For high conductivity ratios ($\kappa << 1$) and if N is of order 10^{-1}, Equation 28 reduces to $\beta = 1$. The *shifted concentration gradient* $\Delta c/\Delta x$in Equation 26 represents the mass that is shifted by the advective transport through each domain A. It is not considered to be a driving force as it is in the common, similar expression for diffusive or Fickian dispersion.

The dispersive mass flux (f) in Equation 26 is affected by the four parameters used to describe ω in Equation 27. In brief, f and ω increase without limits when L_h is increased. In the case of a thin plume, D_p replaces I_h in β_j Equation 28 and $(L_p + L_T)$ replaces L_h in Δs Equation 22 leading to a reduction of the values of f and ω. The ratio N is reciprocally related to D which determines the maximum value of I_h in the case of a high conductivity zone. In a case with a high conductivity zone, a decrease of N will lead to an increase of D, f and ω. The impact of κ on ω is discussed next.

Comparison between the Advective Volume Shift ω and the Dispersivity α

The position of ω in Equation 27 is the same as that of α in Fick's law. Figure 6 shows how α, ω, β, and Δs vary with $\sigma_{\ln(k)}$. As α presumes symmetric spreading, it is shown also for the tail. The parameters values underlying this figure are $L_h = 10$ m, $D_h = 1$ m, $D_p = 1$ m, $\eta = 1$ and $N = 3$, while κ varies along the x-axis.

The values of α and ω behave differently with changing $\sigma_{\ln(k)}$. In highly heterogeneous soils, ω is limited in the front due to the limitation of the spread following from Equation 22. This is caused by the limited velocity inside the conductivity zone and due to a long tail becoming thin, as accounted for in Equation 28. A comparison of Equations 21 and 26 shows that the values of ω and α are about equal if the values of σ and N are about equal in weakly heterogeneous aquifers ($\sigma_{\ln k} < 1$).

Application in Modeling: Adaptation to Cell Size

Both f and ω apply to a length (L) as described in Equation 26. In numerical modeling, longitudinal dispersion is 1D in the direction of flow. The cell size determines the path length X [m] over which dispersion or spread occurs in a cell and should be accounted for in that cell. In a cell with size X, this spread occurs X/L

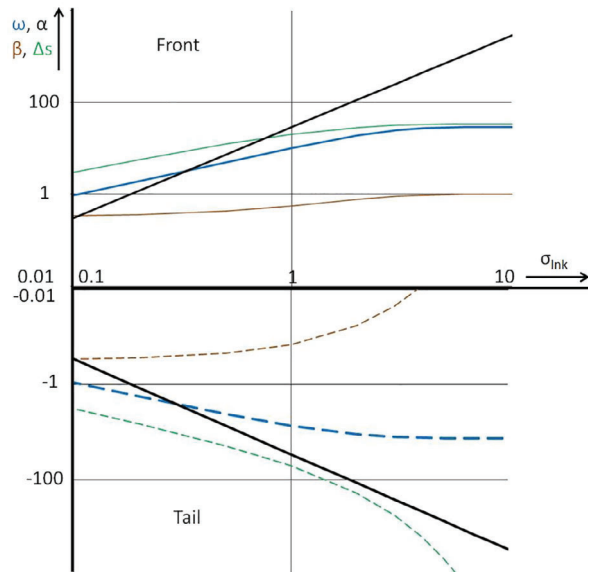

Figure 6. Variation α (black), ω (blue), β (brown) and Δs (green) with $\sigma_{ln(k)}$ for front and tail.

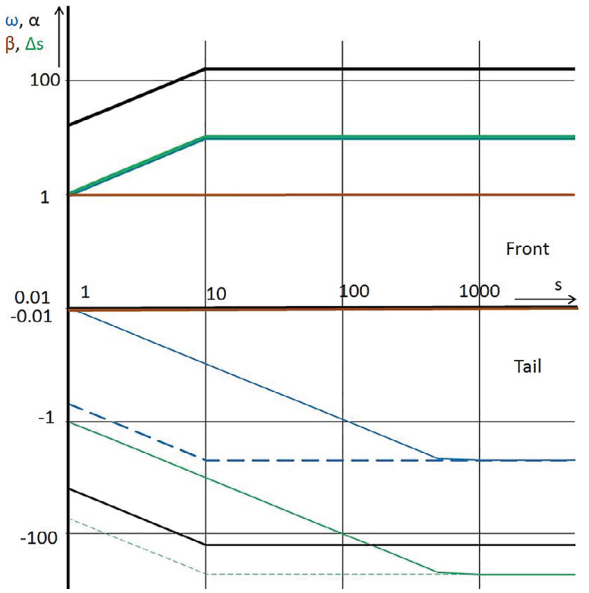

Figure 7. Variation of α (black), ω (blue), β (brown) and Δs (green) with s for $\sigma_{ln(k)} = 4$; dotted lines denote computed values without correction for $\Delta s > s$.

times in which case the 1D dispersive mass flux in a cell f_{cell} becomes:

$$F_{cell,j} = F_j\big|_L \frac{X}{L} = \omega_{cell,j} \frac{\Delta c}{\Delta x} u_a \qquad (29)$$

So:

$$\omega_{cell,j} = \omega_j X/L \qquad (30)$$

The parameter ω_{cell} is called the *cell advective volume shift* and is proportional to the cell size. Because of the similarity between ω and α in the expression for the mass flux, Equation 30 might also apply to α. The ratio X/L may give support to the common practice of using large dispersivities in large models because of the use of large cells rather than the travel distance.

Discussion

In field experiments such as those at Borden (Rajaram and Gelhar 1991), Cape Cod (Hess et al. 2002), and MADE (Adams and Gelhar 1992), travel distance is often not sufficient to fulfill ergodicity and the plume development is strongly asymmetric. The present theory enables engineers to quantify the transport phenomena as they occur to a plume passing through a single conductivity zone as it travels in a heterogeneous aquifer. Dispersion at this scale has a strong advective transport component and is hardly Fickian. The limited growth in the plume front and the growth of the tail over a long distance causes asymmetric deformation of the plume, contrary to the results from Fickian dispersion.

The value of ω can strongly differ with travel distance s from that of α, especially in highly heterogeneous aquifers as illustrated in Figure 7 which shows α, β, Δs, and ω varying with s when $\sigma_{ln(k)} = 4$. The underlying parameters are the same as those used in Figure 6. For path lengths shorter than L_h, Δs increases linearly with a distance that follows from Equation 22. It is known (Gelhar 1993) that α increases approximately linearly in the initial spreading phase, which is assumed to occur over the length L_h in this comparison. The spread in the tail calculated from Equation 22 is larger than the path length over the first 500 m. The path length then determines the actual spread and reduction of ω.

Porosity differences matter in dispersion because they affect the velocities of water particles with dissolved mass. For instance, in a zone with low porosity where the conductivity is equal to that of the aquifer, the Darcy velocity is equal inside and outside but the water particles travel faster inside than outside. When the water particles then leave the zone, they become adjacent to water particles having traveled slower outside the zone, causing dispersion to occur. Porosity is known to be relevant to dispersion (Konikow 2011). Because large pores between cobbles are often filled with smaller grains, porosity generally decreases with increasing conductivity, strengthening dispersion (see table 2.1 from Dominico and Schwarz (1990)). This relation is opposite to that described without proof by Dagan and Lessoff (2001). For field situations, Gelhar (1997) mentioned that "porosity differences easily can account for differences between the observed geometric mean and the effective hydraulic conductivity derived from the velocity of the center of the mass in the field experiments of Borden (Sudicky 1986)." The porosity ratio is significant in transport calculations when $\kappa \leq \eta$ and vanishes when κ is high, which is also mentioned by Lessoff and Dagan (2001).

Conclusions

The present theory enables engineers to quantify the advective transport phenomena that underlie

non-ergodic and asymmetric dispersion. These phenomena occur at macro scale to a plume as it passes through a single conductivity zone. Simple expressions describe the spread of water particles in that plume, the thickness of the bundle of flowlines entering and leaving the zone (the wake), the lengths of the zones of inflow, outflow and through-flow, the ratio between the forward and backward part of the shift of water particles in the plume, and the reduction to particle spreading when a plume is relatively thin.

Asymmetric dispersion is caused by the different spreads of the front and tail of a plume. These spreads can be calculated by using the high and low conductivity values at the standard deviation in the log conductivity distribution, which are substituted in the simple expression for the spread (in the case of a single conductivity zone) or for the standard deviation (in the case of a heterogeneous aquifer).

The spread derived from a spatial distribution in a field experiment can be interpreted as the geometric mean of the spreads of the front and tail of the plume.

Break-through measurements in field experiments apply to a thin part of the injected plume which is often inside a conductivity zone. In this case, an expression is presented to scale up the spread that is representative of the overall aquifer.

The fundamentally new expression for the dispersive mass flux represents advective transport phenomena only. In this Fickian-like expression, the advective volume shift ω replaces the classic dispersivity α and the concentration gradient is a measure of the mass that is shifted instead of being the driving force. The advective volume shift ω equals the spread of the front (or tail) of the plume multiplied by the wake fraction. The wake fraction accounts for a long tail being thin.

The advective volume shift is a function of the cell size. The similarity between the new expression for the dispersive mass flux and Fick's law may give support to the common practice of using large dispersivities in large models.

Acknowledgment

The support in discussions and writing by Dr. Theo N. Olsthoorn, professor emeritus at Delft University of Technology, has led to considerable improvement of the manuscript. Many persons have supported the author along the road to the present work over the last 25 years in different ways and at different levels. They all are gratefully acknowledged.

Author's Note

The author does not have any conflicts of interest or financial disclosures to report.

References

Adams, E.E., and L.W. Gelhar. 1992. Field study of dispersion in a heterogeneous aquifer: 2. Spatial moments analysis. *Water Resources Research* 28: 15.

Appelo, C.A.J., and D. Postma. 1993. *Geochemistry, Groundwater and Pollution*. Rotterdam, The Netherlands: A.A. Balkema.

Batu, V. 2006. *Applied Flow and Solute Transport Modeling in Aquifers*. Boca Raton, Florida: Taylor & Francis.

Bear, J.A., and A. Verruijt. 1987. *Modeling Groundwater Flow and Pollution*. Dordrecht, The Netherlands: D. Reidel Publishing Company.

Dagan, G., and S.C. Lessoff. 2001. Solute transport in heterogeneous formations of bimodal conductivity distribution: 1. Theory. *Water Resources Research* 37: 465–472.

De Lange, W.J. 1996. *Groundwater Modeling of Large Domains Using Analytic Elements*. Delft: Delft University of Technology.

Dominico, P.A., and F.W. Schwarz. 1990. *Physical and Chemical Hydrogeology*. New York: John Wiley and Sons.

Eames, I., and J.W.M. Bush. 1999. Longitudinal dispersion by bodies fixed in a potential flow. *Proceedings: Mathematical, Physical and Engineering Sciences* 455: 3665–3686. https://doi.org/10.1098/rspa.1999.0471

Feehley, C.E., C. Zheng, and F.J. Molz. 2000. A dual-domain mass transfer approach for modeling solute transport in heterogeneous aquifers: Application to the macrodispersion experiment (MADE) site. *Water Resources Research* 36: 2501–2515. https://doi.org/10.1029/2000WR900148

Fiori, A., I. Jankovic, and G. Dagan. 2003. Flow and transport in highly heterogeneous formations: 2. Semi-analytical results for isotropic media. *Water Resources Research* 39: 1–9. https://doi.org/10.1029/2002WR001719

Fiori, A., I. Janković, and G. Dagan. 2006. Modeling flow and transport in highly heterogeneous three-dimensional aquifers: Ergodicity, Gaussianity, and anomalous behavior—2. Approximate semianalytical solution. *Water Resources Research* 42: 1–10. https://doi.org/10.1029/2005WR004752

Fiori, A., G. Dagan, I. Jankovic, and A. Zarlenga. 2013. The plume spreading in the MADE transport experiment : Could it be predicted by stochastic models? *Water Resources Research* 49: 2497–2507. https://doi.org/10.1002/wrcr.20128

Fiori, A., A. Zarlenga, I. Jankovic, and G. Dagan. 2017. Solute transport in aquifers: The comeback of the advection dispersion equation and the first order approximation. *Advances in Water Resources* 110: 349–359. https://doi.org/10.1016/j.advwatres.2017.10.025

Fiori, A., V. Cvetkovic, G. Dagan, S. Attinger, A. Bellin, P. Dietrich, A. Zech, and G. Teutsch. 2016. Debates–Stochastic subsurface hydrology from theory to practice: The relevance of stochastic subsurface hydrology to practical problems of contaminant transport and remediation. What is characterization and stochastic theory good for? *Water Resources Research* 52, no. 12: 9228–9234. https://doi.org/10.1002/2015WR017525

Gelhar, L.W. 1993. *Stochastic subsurface hydrology*. Englewood Cliffs, NJ: Prentice Hall Inc.

Gelhar, L.W. 1997. Perspectives on field-scale application of stochastic subsurface hydrology. In *Subsurface Flow and Transport: A Stochastic Approach*, ed. G. Dagan and S.P. Neuman. Cambridge, UK: Cambridge University Press.

Gelhar, L.W., and C.L. Axness. 1983. Three-dimensional stochastic analysis of macrodispersion in aquifer. *Water Resources Research* 19: 20.

Hadley, P.W., and C. Newell. 2014. The new potential for understanding groundwater contaminant transport. *Groundwater* 52: 174–186. https://doi.org/10.1111/gwat.12135

Heinz, J., and T. Aigner. 2003. Hierarchical dynamic stratigraphy in various quaternary gravel deposits, Rhine glacier area (SW Germany): Implications for hydrostratigraphy. *International Journal of Earth Sciences* 92: 923–938. https://doi.org/10.1007/s00531-003-0359-2

Hess, K.M., J.A. Davis, D.B. Kent, and J.A. Coston. 2002. Multispecies reactive tracer test in an aquifer with spatially variable chemical conditions, Cape Cod, Massachusetts: Dispersive transport of bromide and nickel. *Water Resources Research* 38: 36-1–36-17.

Jankovic, I., A. Fiori, and G. Dagan. 2003. Flow and transport in highly heterogeneous formations: 3. Numerical simulations and comparison with theoretical results. *Water Resources Research* 39, no. 9: 1270. https://doi.org/10.1029/2002WR001721.

Jensen, K.H., K. Bitsch, and P.L. Bjerg. 1993. Large-scale dispersion experiments in a Sandy aquifer in Denmark: Observed tracer movements and numerical analyses. *Water Resources Research* 29: 24.

Konikow, L.F. 2011. The secret to successful solute-transport modeling. *Ground Water* 49: 144–159. https://doi.org/10.1111/j.1745-6584.2010.00764.x

Lessoff, S.C., and G. Dagan. 2001. Solute transport in heterogeneous formations of bimodal conductivity distribution: 2. Applications. *Water Resources Research* 37: 473–480.

Molz, F. 2015. Advection, dispersion, and confusion. *Groundwater* 53: 348–353. https://doi.org/10.1111/gwat.12338

Neuman, S.P. 2014. The new potential for understanding groundwater contaminant transport. *Groundwater* 52: 653–656. https://doi.org/10.1111/gwat.12245

Neuman, S.P., and D.M. Tartakovsky. 2009. Perspective on theories of non-Fickian transport in heterogeneous media. *Advances in Water Resources* 32: 670–680. https://doi.org/10.1016/j.advwatres.2008.08.005

Ptak, T., and G. Teutsch. 1994. Forced and natural gradient tracer tests in a highly heterogeneous porous aquifer, instrumentation and measurements. *Journal of Hydrology* 159: 79–104. https://doi.org/10.1016/0022-1694(94)90250-X

Rajaram, H., and L.W. Gelhar. 1991. Three-dimensional spatial moments analysis of the Borden Tracer Test. *Water Resources Research* 27: 1239–1251.

Rehfeld, K.R., K.M. Boggs, and L.W. Gelhar. 1992. Field study of dispersion in a heterogeneous aquifer, 3. Geostatistical analysis of hydraulic conductivity. *Water Resources Research* 28: 16.

Strack, O.D.L. 1981. *Assessment of Effectiveness of Geologic Isolation Systems; Analytic Modeling of Flow in Fissured Medium*. Richmond, Washington: Pacific Northwest Lab.

Strack, O.D.L. 1989. *Groundwater Mechanics*. New Jersey: Prentice Hall Inc.

Sudicky, E.A. 1986. Natural gradient experiment on solute transport in a sand aquifer: Spatial variability of hydraulic conductivity and its role in the dispersion process. *Water Resources Research* 22: 14.

Theis, C.V. 1967. Aquifers and models. In *Proceedings of Symposium on Groundwater Hydrology*, American Water Resources Association, 138.

Westerhof, W. 2009. Stratigraphy and sedimantary evolution: The lower Rhine-Meuse system during the Late Pliocene and early Pleistocene (southern North Sea Basin). TNO Geological Survey of The Netherlands, Utrecht.

Zheng, C., and P.P. Wang. 1999. MT3DMS: A modular three-dimensional multispecies transport model for simulation of advection, dispersion and chemical reactions of contaminants in groundwater systems. Documentation and User's Guide.